JACS
JOURNAL OF THE AMERICAN CHEMICAL SOCIETY

Article

pubs.acs.org/JACS

Impact of G12 Mutations on the Structure of K-Ras Probed by Ultraviolet Photodissociation Mass Spectrometry

Michael B. Cammarata,[†] Christopher L. Schardon,[‡] M. Rachel Mehaffey,[†] Jake Rosenberg,[†] Jonathan Singleton,[†] Walter Fast,[§] and Jennifer S. Brodbelt*[,†]

[†]Department of Chemistry, [‡]Graduate Program in Biochemistry, and [§]Division of Chemical Biology and Medicinal Chemistry, College of Pharmacy, University of Texas, Austin, Texas 78712, United States

Supporting Information

ABSTRACT: Single-residue mutations at Gly12 (G12X) in the GTP-ase protein K-Ras can lead to activation of different downstream signaling pathways, depending on the identity of the mutation, through a poorly defined mechanism. Herein, native mass spectrometry combined with top-down ultraviolet photodissociation (UVPD) was employed to investigate the structural changes occurring from G12X mutations of K-Ras. Complexes between K-Ras or the G12X mutants and guanosine 5′-diphosphate (GDP) or GDPnP (a stable GTP analogue) were transferred to the gas phase by nano-electrospray ionization and characterized using UVPD. Variations in the efficiencies of backbone cleavages were observed upon substitution of GDPnP for GDP as well as for the G12X mutants relative to wild-type K-Ras. An increase in the fragmentation efficiency in the segment containing the first 50 residues was observed for the K-Ras/GDPnP complexes relative to the K-Ras/GDP complexes, whereas a decrease in fragmentation efficiency occurred in the segment containing the last 100 residues. Within these general regions, the specific residues at which changes in fragmentation efficiency occurred correspond to the phosphate and guanine binding regions, respectively, and are indicative of a change in the binding motif upon replacement of the ligand (GDP versus GDPnP). Notably, unique changes in UVPD were observed for each G12X mutant with the cysteine and serine mutations exhibiting similar UVPD changes whereas the valine mutation was significantly different. These findings suggest a mechanism that links the identity of the G12X substitution to different downstream effects through long-range conformational or dynamic effects as detected by variations in UVPD fragmentation.

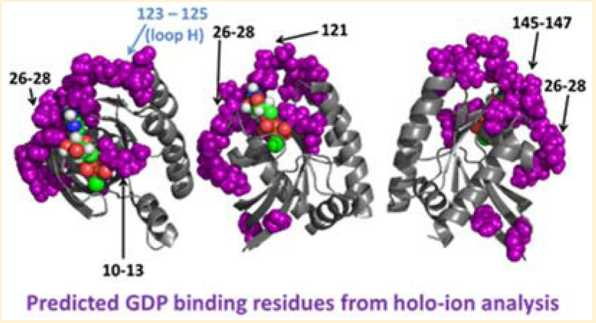

INTRODUCTION

Proteins containing single amino acid mutations (presumably arising from somatic mutations acquired in a given cell over time) are expressed in a large number of cancerous tissues.[1,2] These mutations can specifically modulate the function of the protein in question, a factor which may promote cancer growth.[2] For example, single point mutations leading to constitutively active members of the rat sarcoma (Ras) family of proteins have been implicated in cell cycle progression, proliferation, apoptosis, and senescence, all important in cancer.[3] Within the Ras family of proteins, K-Ras is the most frequently mutated isoform, present in 22% of all tumors analyzed and 90% of pancreatic tumors.[4] Of the point mutations found in K-Ras, 80% are found at codon 12. At this amino acid position—a Gly in wild-type (WT) K-Ras—mutations that introduce larger side chains block the ability of GTPase activating protein (GAP) to stimulate K-Ras hydrolysis of guanosine triphosphate (GTP), thereby locking it into an active state. Trapping the K-Ras protein in an active state leads to abnormally high concentrations of GTP-bound K-Ras, which results in up-regulation of downstream pathways and unregulated cell proliferation and tumor growth. The particular amino acid substitutions found at the G12 position (designated here by G12X) vary in frequency, with G12D being the most prevalent, followed by G12V, G12C, and others. These substitutions also vary in frequency by cancer type.[4] For example, the G12D mutation is often found in colon, lung, pancreatic, and skin cancer tissues, among others. The G12V mutation is also widespread but can show greater prevalence than G12D in skin cancers. The G12C mutation is extremely prevalent in lung cancers, and other G12X mutations, such as G12S, appear less frequently.[4] In addition to differences in distribution by cancer type, the identity of the side-chain substitution at G12X leads to different downstream functional effects (vide infra) through a mechanism that is not well defined. Therefore, development of novel tools for investigating how particular mutations affect the conformation and binding interactions of K-Ras in particular, and other disease-relevant proteins in general, would be a compelling advance.

Received: October 28, 2015
Revised: April 30, 2016
Published: September 25, 2016

DOI: 10.1021/jacs.6b04474
J. Am. Chem. Soc. 2016, 138, 13187−13196

In recent years, mass spectrometry (MS) has become an increasingly popular approach for addressing a variety of questions in the arena of structural biology.[5−7] Strategies using chemical probes, including hydrogen/deuterium exchange (HDX) methods and other covalent-labeling methods, to evaluate solvent accessibilities and map protein interfaces have played a prominent role in advancing the applications of tandem mass spectrometry (MS/MS) for studying structures of proteins.[8−12] While chemical probe methods have been applied with great success, the use of top-down MS to examine native-like intact proteins and protein complexes has accelerated, especially with advances in MS/MS methods that are sensitive to protein structure. Native MS involves the use of buffered spray solutions containing volatile salts, typically ammonium acetate, which allows gentle transfer of proteins into the gas phase in low charge states (compared to proteins ionized using conventional nanospray conditions).[13−17] Although there are unresolved questions about the specific mechanisms of native electrospray ionization (ESI), in favorable cases the charged proteins remain to a large extent folded, similar to the tertiary and quaternary structures adopted in solution.[18−22] The shapes of proteins ionized by native ESI have been evaluated successfully by ion mobility MS, in which the measured collisional cross sections have been correlated with the sizes of native proteins in solution, thus providing evidence that the proteins remain native-like during their transfer to the gas phase.[23−26] Cross sections of proteins obtained from ion mobility measurements have been shown to increase significantly with charge state, thus signaling their unfolding.[18] Native MS has gained additional momentum with the growing availability of high-resolution/high-mass-accuracy mass spectrometers that have allowed greater implementation of MS/MS methods for analysis of intact proteins.[27] To date, native MS has been applied to a large array of applications in structural biology, including examination of stoichiometries of protein complexes, ligand binding, binding/dissociation constants, conformational changes of proteins, and dynamic unfolding.[13−17,25−33]

With respect to MS/MS characterization of native-like proteins and protein complexes, electron-based activation methods, such as electron transfer dissociation (ETD)[34] and electron capture dissociation (ECD),[31,35−38] provide significant diagnostic sequence information. The abundances of the resulting fragments have been correlated with the degree of flexibility of different regions of the proteins, thus reflecting crystallographic B-factors.[31,37,39] Salt bridges in proteins may survive upon electron-transfer reactions, resulting in electron transfer but without dissociation of the resulting fragments, and the proteins release the electrostatically bound fragment ions upon further activation.[34] Another activation technique, surface-induced dissociation (SID), has proven to be particularly impressive for determination of quaternary arrangements of native multi-protein complexes.[40,41] A third method takes advantage of high-energy excitation via absorption of 193 nm photons to give the most extensive backbone fragmentation of proteins by any activation method.[42,43] Ultraviolet photodissociation (UVPD) has shown unprecedented sequence coverage for unfolded proteins as well as their natively ionized analogues.[30,32,33,44] Additionally, the patterns of backbone cleavages promoted by UVPD not only correlate with the average B-factors of residues in proteins (which can reflect thermodynamic motions and/or heterogeneity of the crystal lattice among other factors) but also reveal ligand binding sites based on suppression or enhancement of fragmentation and retention of the ligand by the fragment ions upon protein dissociation.[30,33] The variations in UVPD fragmentation observed at specific backbone cleavage sites may arise from longer-range changes in protein structure, such as disruptions or changes of secondary or tertiary structural features. This level of detail has not been fully unscrambled but certainly merits further attention as additional protein complexes are evaluated. The UVPD patterns have been shown to be modulated for different gas-phase conformers, as measured by ion mobility MS.[45,46] Most recently, UVPD was used to elucidate ligand binding sites and monitor the conformational changes of dihydrofolate reductase (DHFR) upon binding of co-factor NADPH and its inhibitor methotrexate.[30] At the conclusion of this previous study, it was proposed that UVPD should be tested on a protein with single amino acid mutations to evaluate the sensitivity of UVPD to subtle changes in sequence that might (or might not) cause conformational changes of the protein as well as induce alterations of ligand binding modes,[30] a proposal that catalyzed the present work.

In the present study, native MS and top-down UVPD are used to characterize protein−ligand complexes comprised of WT K-Ras or clinically relevant G12X mutants of K-Ras, including G12C, G12S, and G12V. In our hands, the most common G12D variant was not stable upon purification and thus could not be studied (data not shown). These K-Ras variants are characterized bound to either guanosine diphosphate (GDP) or guanosine 5′-[β,γ-imido]triphosphate (GDPnP), a non-hydrolyzable analogue of guanosine triphosphate (GTP). (The structures of these ligands are shown in Figure S1.) The structural changes upon GTP hydrolysis of WT K-Ras have been studied using conventional biophysical methods such as crystallography,[47] NMR,[48] and HDX[49] and provide a comparative framework for the gas-phase UVPD approach used in the present study. An extensive review has also been published on Ras protein−protein interactions.[50] Building on this work, we then compare variations in UVPD fragmentation of GDP and GDPnP complexes containing WT K-Ras or the G12C, G12S, and G12V variants to decipher unique structural changes arising from these single point mutations. Our work highlights structural changes in G12X K-Ras that are distant to the mutation site yet are dependent on the identity of the mutated residue, providing a possible mechanism linking the identity of different substitutions at this position to their differing downstream effects.

EXPERIMENTAL SECTION

Protein Expression and Purification. Recombinant human wild-type K-Ras (isoform 2, residues 1−169, 18 954 Da) was expressed using previously described expression plasmids[51] and purified as detailed in the Supporting Information. Expression and purification for the G12C, G12S, or G12V variants were the same. Each of the WT, G12C, G12S, or G12V K-Ras variants was further purified by ion-exchange chromatography.

Mass Spectrometry. Equimolar protein/ligand solutions were prepared at a concentration of 15 μM at pH 7.8 buffered with 50 mM ammonium acetate with 5 μM magnesium acetate. The pH was adjusted by addition of ammonium hydroxide. The solutions were infused via a gold-coated static tip operated between 1.5 and 1.7 kV at a capillary temperature of 200 °C. All experiments were performed on a Thermo Scientific Orbitrap Elite mass spectrometer (Bremen, Germany) equipped with a Coherent Excistar 193 nm excimer laser (Santa Cruz, CA) and modified to allow UVPD as described previously.[42] All mass spectra were collected at 240 K resolution at

DOI: 10.1021/jacs.6b04474
J. Am. Chem. Soc. 2016, 138, 13187−13196

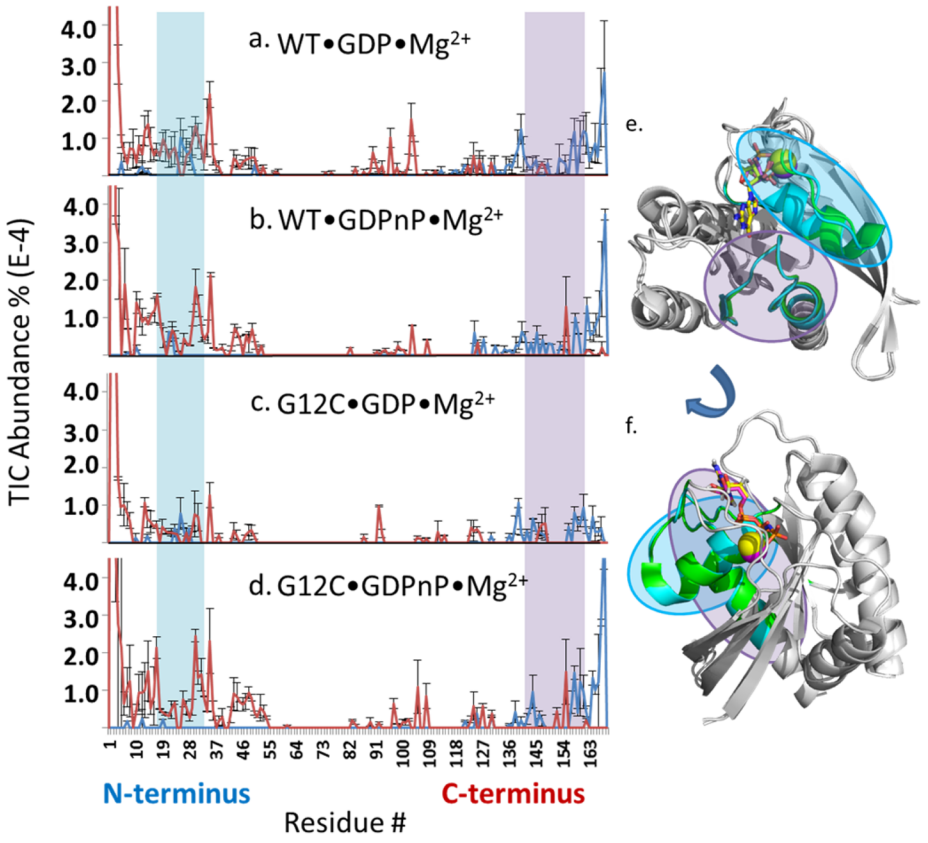

Figure 1. (a–d) Relative abundances of the holo (ligand-containing) fragment ions produced upon UVPD of WT K-Ras and G12C complexes, color coded as N-terminal holo fragments (blue traces) and C-terminal holo fragments (red traces). The UVPD fragment ion maps for the corresponding G12V and G12S complexes are shown in Figure S10. The abundances are plotted relative to the amino acid sequence along the *x*-axis to convey the relative efficiencies of backbone cleavages adjacent to each residue. Shaded regions (blue and lavender shading) highlight the regions of the most notable changes in UVPD fragmentation efficiencies between the GDP and GDPnP complexes and are expanded in Figure S11. (e,f) The same blue and lavender regions are highlighted on a superposition of crystal structures 3GFT (WT K-Ras·GDPnP·Mg^{2+} complex with green for WT K-Ras features and yellow for the GDPnP ligand) and 4OBE (WT K-Ras·GDP·Mg^{2+} complex with turquoise for WT K-Ras features and pink for the GDP ligand). Two rotated views are shown in e and f.

m/*z* 400. Fifty scans were averaged for the MS1 spectra with an automatic gain control (AGC) of 5e5. All UVPD experiments were performed using a single 3 mJ pulse (without focusing or collimation of the laser). The 8+ charge state of each protein or protein/ligand complex was selected for MS/MS analysis, using an isolation width of 12.5 *m*/*z*. The AGC value was set to achieve a signal level of 2e5 with a fill time of 1 s for UVPD experiments. The Orbitrap mass analyzer was scanned from *m*/*z* 220 to 4000, and 750–1000 scans were averaged for each UVPD mass spectrum. Three or four replicates were collected for each protein/ligand complex. Three replicates was standard, but a fourth was collected for cases in which the stability of the spray deteriorated during acquisition of a spectrum.

Data Analysis. The UVPD mass spectra were decharged using Xtract with a signal-to-noise ratio of 2, a fit factor of 44%, and remainder of 25%. The monoisotopic ions were then searched against the respective K-Ras amino acid sequence using a version of Prosight PC 3.0 modified to accommodate UVPD fragmentation. This involves searching for the following ions: a, $a^{\bullet}$, b, c, x, $x^{\bullet}$, y, y − 1, and z. The spectra were also searched by considering all fragment ions with a mass shift corresponding to each ligand mass both with and without the coordinating Mg^{2+}. The more abundant holo (i.e., ligand-containing) fragment ion species contained both the ligand and the coordinated divalent magnesium for both the GTP and GDPnP complexes of each K-Ras variant. GDPnP was used as a stable surrogate of GTP that does not undergo hydrolysis. Specifically, fragment ion searches undertaken for GDP·Mg^{2+} complexes included the mass shift 462.9781–464.9937 Da, and those undertaken for the GDPnP·Mg^{2+} complexes included the mass shift 541.9604–543.9760 Da. All product ions identified upon UVPD of the various K-Ras complexes are summarized in Tables S1–S8. For analysis of backbone cleavage yields upon UVPD, the abundances of the holo fragment ions were collectively summed with the abundances of the corresponding apo ion series (i.e., ligand not retained). All identified ions were normalized to the total ion current of the spectrum to allow direct comparison across all spectra. Identified ions (both apo and holo) from N- and C-terminal ions were summed together as described in Cammarata et al.,[30] unless stated otherwise. In short, fragment ions arising from cleavage of the backbone positions between pairs of adjacent amino acids in the protein sequence were collectively summed. For example, all N-terminal product ions (a_n, b_n, and c_n ions) arising from backbone cleavages that occur C-terminal to a specific amino acid were summed with all the C-terminal product ions (x_{R-n+1}, y_{R-n+1}, and z_{R-n+1} ions) arising from cleavages that occur N-terminal to the same amino acid, where *n* is the residue number and *R* is the total number of amino acids in the protein. This value is calculated for each amino acid to convey the backbone cleavage efficiency adjacent to each particular residue. The determination of statistical significance of a change in backbone cleavage efficiency upon UVPD is described in Figures S2–S4. In brief, Student's *t* test was performed for each comparison of UVPD between WT K-Ras and each variant. Graphs displaying the $t_{calculated}$ values are shown in Figure S4, along with thresholds for the $t_{critical}$ at several different confidence intervals. Crystal structures 4OBE and 3GFT (referring to their Protein Databank IDs) were used for the WT GDP and WT GDPnP models, respectively. Diagrams of the crystal structure (3GFT) of WT K-Ras·

DOI: 10.1021/jacs.6b04474
J. Am. Chem. Soc. 2016, 138, 13187–13196

GDPnP·Mg^{2+} are shown in Figure S5 to illustrate the helices, loops, switches, and β-strands.

RESULTS

Solutions containing each combination of K-Ras protein (WT, G12C, G12V, or G12S) and one ligand (GDP or GDPnP) were infused using nanoESI conditions, and the 8+ charge state was subsequently isolated and subjected to 193 nm UVPD to produce informative fragmentation patterns. A representative ESI mass spectrum is shown in Figure S6a for WT K-Ras, and the characteristic narrow and low charge state distribution (9+, 8+, 7+) is observed. Complexes formed upon addition of GDP or GDPnP to the solutions are displayed in Figure S6b-i, showing the prominent formation of ternary complexes containing the protein, the nucleotide, and divalent magnesium. There are also other sodium, magnesium, and ammonium adducts detected (species that are prevalent in native MS). The 8+ charge state was selected for UVPD owing to its large abundance. Replacement of GDP by GDPnP occurred with about 95% efficiency. Each complex of interest was isolated and activated by UVPD to generate the MS/MS spectra that are shown in Figure S7. The raw UVPD fragmentation patterns were decharged using XTRACT to produce the deconvoluted spectra in Figure S8, with the masses of the fragments extending from very low mass (380 Da) up to 11 000 Da. Assignment of the fragment ions and interpretation of the data entailed analysis of both the apo and holo product ions, as described in the Experimental Section. Complete lists of identified products ions with their theoretical and experimental masses are provided in the Supporting Information. For this analysis, products containing just the nucleotide by itself or containing both the nucleotide and magnesium ion(s) were considered (see Figure S9). On average, 142 GDP·Mg^{2+} unique holo sequence ions and 139 GDPnP·Mg^{2+} unique holo sequence ions were identified for each protein construct. The sequence coverage obtained by UVPD of the GDP complexes was 96%, 96%, 89%, and 76% for WT, G12C, G12V, and G12S, respectively. The coverage obtained for the corresponding GDPnP complexes was 92%, 91%, 86%, and 87% for WT, G12C, G12V, and G12S. The sequence coverage obtained upon UVPD of the 18+ (denatured) charge state of all K-Ras variants was 89%, 80%, 92%, and 85% for WT, G12C, G12V, and G12S, respectively. The decrease in the sequence coverage for the G12S·GDP·Mg^{2+} complex relative to the G12S·GDPnP·Mg^{2+} complex and denatured G12S is peculiar and may indicate a reordering of the charges on the protein or could arise from the overlap of holo sequence ions with apo sequence ions in a way that obscured a number of key diagnostic ions. Comparisons of the resulting fragment abundances from each variant (18+) show they are very similar, with the exception of three fragment ion outliers (Figure S3), thus indicating that the single point mutations do not cause variations in fragmentation for the denatured proteins. Future studies should include control proteins, when possible, which contain null mutations (ones not anticipated to influence structure or function). Comparison of UVPD-MS results for these control proteins relative to ones incorporating key mutations would afford better metrics for false discovery rates and increase confidence in assessment of statistically relevant variations in fragmentation.

UVPD of WT K-Ras Complexes: Analysis of Holo Fragment Ions and Determination of Ligand Binding Sites. Previously it was shown that analysis of the holo (ligand-containing) fragment ions produced upon UVPD of protein−ligand complexes allowed predictions about the ligand binding sites.[30,33] This analysis focused on identification of those stretches of the protein for which both N-terminal and C-terminal holo fragment ions overlapped, thus indicating regions of the protein that interacted with the ligand(s) and retained the ligand during fragmentation of the protein. Holo fragment ion plots for each protein/ligand combination of WT and G12C K-Ras are displayed in Figure 1, and the holo fragment ion plots for the corresponding G12V and G12S complexes are shown in Figure S10 with expansions of selected regions in Figure S11 (for residues 15−30 and 140−160). To aid visualization of the regions demarcated by the holo fragment ions, the residues of particular interest are represented as space-filled models on the crystal structure of the protein, as illustrated for WT-K-Ras·GDP·Mg^{2+} complex in Figure 2 for

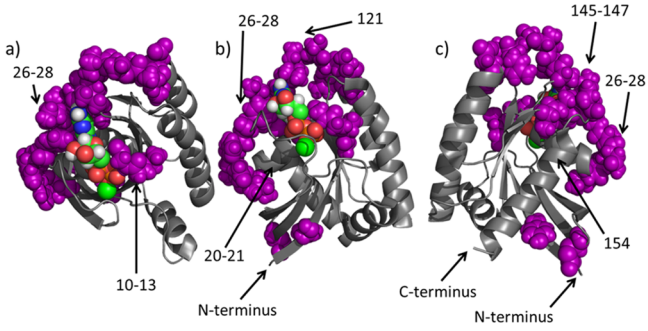

Figure 2. Space-filling models representing potential GDP·Mg^{2+} binding residues derived from the UVPD fragmentation patterns based on detection of holo (GDP-containing) fragment ions from the WT K-Ras·GDP·Mg^{2+} complexes (8+ charge state). The crystal structure represents the GDP-bound WT K-Ras construct (4OBE, WT K-Ras·GDP·Mg^{2+}) displayed as three views (a) top, (b) front side and (c) back side. The purple-colored spheres are residues which are derived from the holo fragment ions. Specific amino acids are numbered in the crystal structures. Multicolored spheres represent the GDP·Mg^{2+}, as follows: blue = nitrogen, green = carbon, red = oxygen, white = hydrogen, orange = phosphorus.

which the key regions are highlighted as purple spheres. For the WT-K-Ras·GDP·Mg^{2+} complex, backbone cleavages at residues 4, 10−13, 26−28, 49, 112, 121, 123−125, and 145−147 resulted in overlapping holo fragment ions from both N and C terminal ions, and these residues are highlighted in Figure 2. The WT-K-Ras·GDP·Mg^{2+} crystal structure (PDB: 4OBE) indicates that residues 13, 15−18, 30, 116−117, 119, and 146 engage in electrostatic interactions with the GDP·Mg^{2+} ligand. The binding sites based on the formation of holo fragment ions from UVPD parallel the predicted location of the ligand. Each amino acid lies within two to three residues of an amino acid known to engage in electrostatic interactions with the ligand, with the exception of sites 4, 49, and 123−125. In many cases the binding sites identified by UVPD are very close to the putative binding sites, but for others it appears that features identified by UVPD may be modulated by structural changes that occur further away, perhaps owing to the influence of longer-range secondary or tertiary structural changes. This may present an opportunity to use the UVPD method to call out structural regions that influence each other in ways that may not be obvious in crystal structures. It is also possible that the holo fragment ions related to these residues arise from

DOI: 10.1021/jacs.6b04474
J. Am. Chem. Soc. 2016, 138, 13187−13196

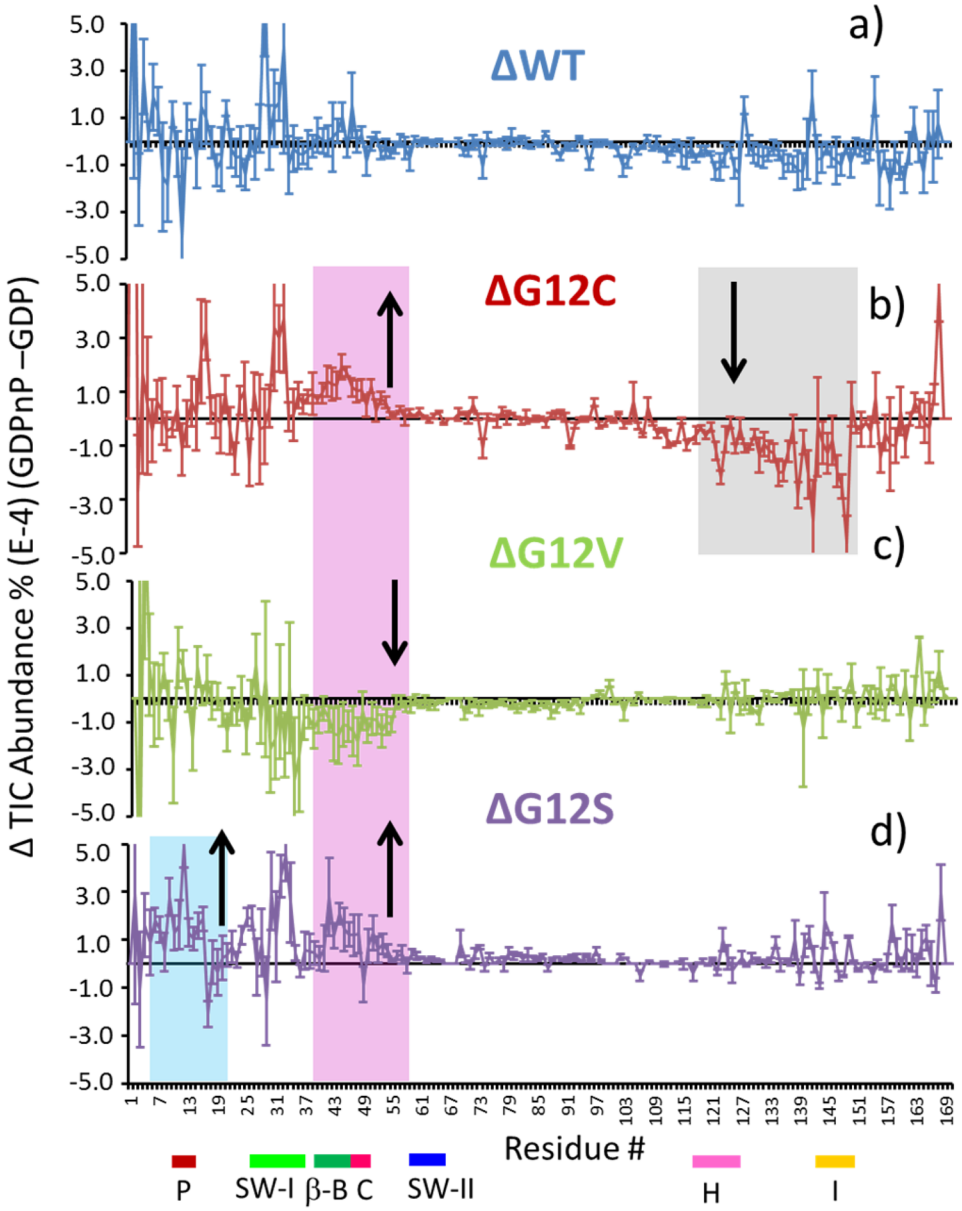

Figure 3. Plots showing the differences in abundances of fragment ions obtained from WT K-Ras and G12X [(a) WT K-Ras, (b) G12C, (c) G12V, and (d) G12S] complexes containing GDPnP or GDP (i.e., differences in abundances of fragment ions from cleavages along the backbone of the protein for each complementary pair of protein·GDP·Mg^{2+} and protein·GDPnP·Mg^{2+} complexes). The difference plots are constructed from the data shown in Figure S12. Upward or downward arrows on the shaded sections indicate those regions for which UVPD is enhanced or suppressed upon ligand exchange from GDP to GDPnP. Relevant loops (P, C, H, I), switches (I, II), and β-strands (B) are labeled underneath the x-axis using colors corresponding to Figure S5.

fragmentation of partially collapsed (non-native) structures in the gas phase, a possibility that deserves further scrutiny.

Evaluation of the holo fragment ions that differ for the K-Ras complexes containing GDP versus GDPnP offers insight into changes in the ligand binding mode as a function of the ligand identity. Two major changes are observed in the graphical displays shown Figure 1 (comparison of Figure 1a (WT K-Ras · GDP·Mg^{2+}) to Figure 1b (WT K-Ras·GDPnP·Mg^{2+}), and comparison of Figure 1c (G12C·GDP·Mg^{2+}) to Figure 1d (G12C·GDPnP·Mg^{2+})). Similar plots are displayed in Figure S10 for complexes containing the G12V and G12S variants. The key regions of the UVPD data from residues 15−30 (shaded in blue in Figure 1) and 140−160 (shaded in lavender in Figure 1) are expanded in Figure S11 for all variants. The first change is noted in the shift of N-terminal ions in the stretch of amino acids around 20−28 for both the WT K-Ras and G12C complexes. N-terminal holo ions arising from backbone cleavages adjacent to residues 24−28 are observed for the GDP complexes, but these N-terminal ions vanish for the GDPnP complexes and instead new N-terminal holo ions that originate from cleavages adjacent to residues 20−21 are observed. The second change is related to the formation of C-terminal holo ions in the region spanning residues 145−154 for the WT K-Ras, G12C and G12V complexes. C-terminal holo ions stemming from backbone cleavages adjacent to residues 145−147 are observed for the GDP complexes, but instead C-terminal holo ions that arise from cleavage adjacent to residue 154 are observed for the GDPnP complexes. We

DOI: 10.1021/jacs.6b04474
J. Am. Chem. Soc. 2016, 138, 13187−13196

attribute these changes in the UVPD behavior to an alteration of the protein conformation that modulates the rigidity/flexibility of those local regions. The implication is that the change in protein conformation arises from a shift in the ligand binding mode of both the phosphate portion and the guanine binding region in the WT K-Ras, G12C, and G12V complexes on going from GDP to GDPnP. Furthermore, when these two general regions (spanning residues 15−30 and 140−160) are superimposed on the crystal structures (4OBE for the K-Ras·GDP·Mg^{2+} complexes and 3GFT for the K-Ras·GDPnP·Mg^{2+} complex), they appear to interact with one another (Figure 1e,f), supporting the idea of a change in the binding motif upon substitution of GDPnP for GDP.

Changes in UVPD Fragmentation upon Ligand Exchange: Impact of GDP versus GDPnP for WT K-Ras. While analysis of the holo fragment ions upon UVPD reveals information about the ligand binding sites as described above, analysis of the combined holo and apo fragment ions provides information about the efficiency of backbone cleavage across the protein, a factor that provides conformational information.[30,32] Backbone cleavages are enhanced or suppressed upon UVPD depending on the flexibility/accessibility of different regions as well as whether those regions are shielded by a ligand (i.e., involved in binding interactions with the ligand) or engaged in other stabilizing intramolecular interactions.[30,32] We were particularly interested in evaluating the changes in backbone fragmentation relative to the impact of the ligand: GDP versus GDPnP. Exchanging the diphosphate nucleotide (GDP) for the triphosphate surrogate (GDPnP) altered the efficiency of backbone cleavage between different residues, as shown in Figure S12 for which the backbone cleavage efficiency upon UVPD is graphically displayed relative to each amino acid in the protein. Major similarities in the UVPD behavior of the GDP versus GDPnP complexes for all four proteins include an enhancement of backbone cleavage in the switch I region and suppression of backbone cleavages in loop H (116−125), loop I (143−150), and the P-loop (10−14). Each of these regions is known to interact directly with the nucleotide ligand.

The visualization of the similarities and differences related to binding GDP versus GDPnP are enhanced via construction of difference plots which are displayed in Figure 3 (protein·GDP·Mg^{2+} versus protein·GDPnP·Mg^{2+}). There are reproducible variations in backbone cleavage efficiency upon UVPD for several regions with respect to WT K-Ras—particularly related to amino acids 1, 3, 5, 6, 9, 15, 16, 20, 28, 30−32, 44, 46, 127, 141, and 154 for which backbone cleavage efficiencies increase for the GDPnP complexes relative to the GDP complexes and residues 2, 7, 8, 11, 18, 24, 73, 102, 121, 122, 125, 126, 138, 139, 147, 155, 157, 159, 160, and 164 for which backbone cleavages decrease for the GDPnP complexes relative to the GDP complexes. The UVPD fragmentation trends are expanded for these regions in Figure 4, and the residues are highlighted on the structure of WT K-Ras in Figure 5 for which blue-colored residues designate a reduction in backbone cleavage (suggesting ligand shielding or involvement in new intramolecular interactions) and red-colored residues denote an increase in backbone cleavage (suggesting greater flexibility or weakened intramolecular interactions) for the GDP versus GDPnP complexes. Considering all constructs analyzed, most of the enhancement in backbone cleavages for the GDPnP complexes occurs in the first 50 residues of K-Ras, whereas most of the suppression occurs beyond residue 100. We speculate that the observed variations reflect the interplay

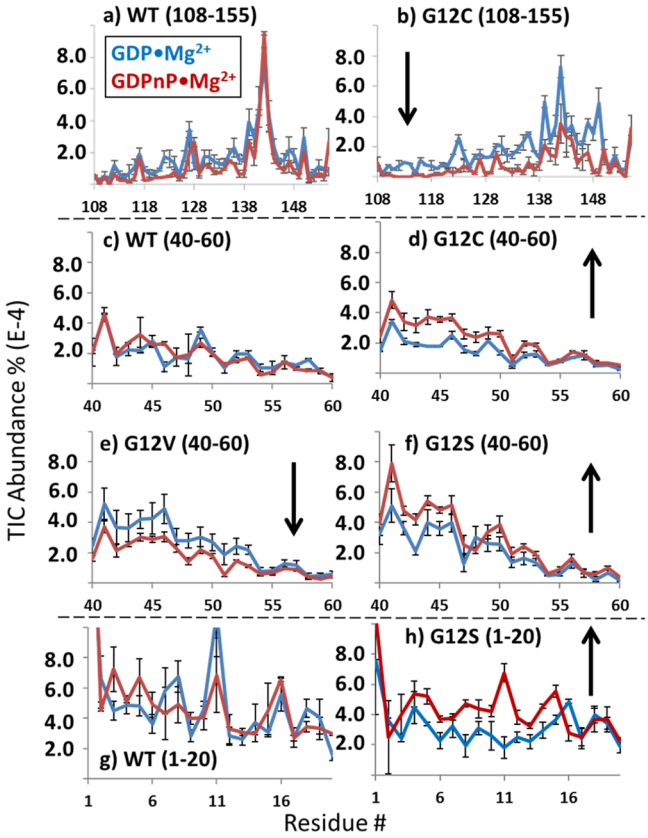

Figure 4. Expansions of UVPD fragmentation trends (from Figure 3) for specific regions along the backbone, particularly (a,b) residues 108−155 for WT K-Ras and the G12C mutant, (c−f) residues 40−60 for all four K-Ras proteins, and (g,h) residues 1−20 of WT K-Ras and the G12S mutant. The complete sets of UVPD fragmentation trends for summed holo and apo fragment ions are shown in Figure 3. The UVPD fragmentation trends are shown in blue for the GDP·Mg^{2+} complexes and red for the GDPnP·Mg^{2+} complexes. Upward or downward arrows indicate those regions for which UVPD is enhanced (upward) or suppressed (downward) upon ligand exchange from GDP to GDPnP, averaging over the entire section of amino acids in that region.

between the known guanine-binding residues (116, 119, 146), the ribose-binding residues (30, 117) and the diphosphate-binding residues (13, 15−18) of the complexes.

UVPD of WT K-Ras versus G12X Complexes: Effects of G12C, G12V, and G12S Mutations. There are also several distinctive differences in the UVPD behavior that specifically point to the impact of the G12X mutations as well as ones related to exchange of GDP for GDPnP. This finding is particularly notable because the mechanism is not clear for how different residue substitutions at the G12 position lead to different downstream effects. Differences upon ligand and/or residue substitutions are highlighted in Figures 3, 4, and S12 for three distinct regions of the proteins along with their general trend of enhanced or suppressed UVPD (upward or downward arrows). The regions of particular interest are comprised of residues 5−20 (shaded in blue in Figure 3d), residues 40−60 (shaded in pink in Figure 3b−d) and residues 120−150 (shaded in gray in Figure 3b). Interestingly, the region spanning residues 40−60 displayed significant changes in UVPD fragmentation for all three mutants (G12C, G12V, G12S) compared to WT K-Ras (Figure 4c−f). UVPD fragmentation was enhanced across the region covering

DOI: 10.1021/jacs.6b04474
J. Am. Chem. Soc. 2016, 138, 13187−13196

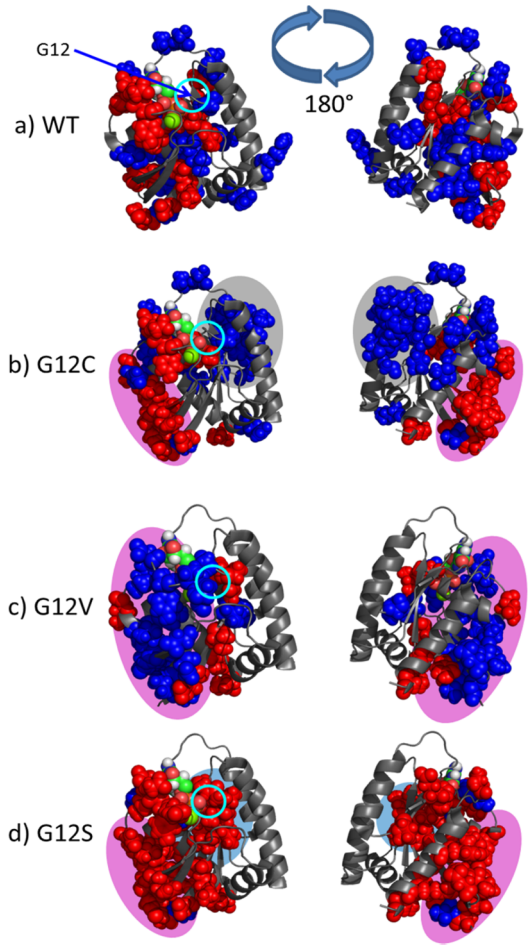

Figure 5. Space-filling models showing the suppression (blue residues) or enhancement (red residues) of backbone cleavages upon UVPD relative to ligand replacement (GDP versus GDPnP) for complexes containing (a) WT K-Ras, (b) G12C, (c) G12V, or (d) G12S constructs. The crystal structure represents the GDP-bound WT K-Ras construct from 4OBE. Regions shaded in light blue (residues 1−20), pink (residues 40−60), and gray (residues 120−150) correspond to the same regions shaded in Figure 3, which indicate regions of change specific to the G12X complexes. The cyan circle indicates the position of the G12 residue in each model.

residues 41−50 after ligand exchange of the G12C and G12S complexes. However, UVPD fragmentation was suppressed in this same region for the G12V complexes. The G12C complexes uniquely exhibited suppression of backbone cleavages for a large portion of the C-terminus region (residues 108−150; the stretch shaded in gray in Figure 3b and expanded in Figure 4b) (comparing the GDP to GDPnP complexes). UVPD of the G12S complexes reveals a unique and significant enhancement in the P-loop (residues 10−14) (shaded in blue in Figure 3d and expanded in Figure 4h). A table of all residues for which UVPD is enhanced or suppressed for each construct is included in Table S9.

DISCUSSION

Analysis of the UVPD trends suggests that, upon exchange of GDP for GDPnP, the guanine-binding region interacts more closely with GDPnP (tighter binding; decreased backbone cleavage upon UVPD), whereas the phosphate-binding and ribose-binding regions become more dynamic (weaker interactions with GDPnP; increased backbone cleavage upon UVPD). This hypothesis is further supported by the earlier observations that the abundances of the N-terminal holo fragment ions (i.e., ones associated with cleavages adjacent to residues 14−22) decreased significantly in the phosphate-binding region (Figure 1) going from the GDP to GDPnP complexes. This results suggests reorientation of this stretch of the protein.

A recent study compared the rates of hydrogen/deuterium exchange (HDX) for WT K-Ras and G12C complexes containing GDP or GDPnP.[49] While these experiments did not allow resolution of HDX rates of individual residues, it was determined that regions encompassing residues 7−19 and 114−120 exchanged at faster rates upon GDPnP ligation, an outcome suggestive of a more open conformation for the GDPnP complexes than the corresponding GDP-bound complexes.[49] These same two regions (7−19 and 114−120) also exhibit considerable changes in backbone cleavage efficiencies upon UVPD in the present study, thus further supporting that the tertiary structures of the proteins in solution are retained in the gas phase. In the same HDX study, one region of K-Ras underwent a slower rate of HDX upon GDPnP ligation (residues 38−52).[49] This region encapsulates the region noted in the present study for which there is a unique change in backbone cleavage upon UVPD for the G12X constructs (containing loop C and strand B, residues 37−49). Although the change in the rate of HDX was small, the underpinning of the conformational structural change may be further exaggerated upon transfer of the protein to the gas phase from solution or may signify a greater sensitivity of UVPD to small conformational changes. The similar findings of these two techniques underscore the feasibility of applying UVPD-MS for characterizing structural changes upon perturbations such as ligand binding (above) and residue substitution (below).

The commonalties and differences in UVPD fragmentation trends with respect to the identity of the amino acid in position 12 (G, C, V, S) are striking. UVPD was enhanced in the region spanning residues 40 to 50 when position 12 was occupied by small polar amino acids that can form hydrogen bonds (C and S), whereas UVPD was suppressed when V, a bulky hydrophobic residue, was located at position 12. Since the G12 position is located at the surface of the protein, it was not obvious or expected that such long-range changes in protein structure would be detected that would be unique to the identity of the substitution at this position. The fact that the presence of these single mutations alters the observed fragmentation behaviors differently reflects the exceptional sensitivity of UVPD to variations in protein structure and is consistent with the hypothesis that the identity of the particular substitution at the G12 position matters with respect to changes in protein structure or dynamics, with possible downstream functional effects that could impact the disease phenotype.

As was demonstrated in the homologue H-Ras (93% amino acid identity to K-Ras residues 1−166), mutation of the G12 site to any amino acid (except Pro) was found to produce an activated H-Ras.[52] The G12 site is situated within van der Waals distance of two residues that stimulate GTP hydrolysis in the complex formed between H-Ras and the GTPase-activating protein p120GAP, so bulkier substitutions at the G12 position would be expected to inhibit GTP hydrolysis, providing a molecular mechanism to explain H-Ras activation.[53] However, not all biological effects are readily explained by an increase in

DOI: 10.1021/jacs.6b04474
J. Am. Chem. Soc. 2016, 138, 13187−13196

the proportion of Ras found in an activated state. For example, the particular identity of the amino acid substituted at the G12 site of H-Ras impacts the morphological phenotype of cells transformed with the corresponding genes.[52] Since the G12 position is on the surface of the protein, the mechanism is unclear for how different substitutions, which are all expected to block GTPase-activating proteins, would lead to different downstream effects. Specifically for K-Ras, G12V and G12D variants were shown to generate distinct differences in the (phospho)proteomic signatures of colorectal cancer cell lines.[54] Additionally, studies in a non-small-cell lung carcinoma cell line showed K-Ras G12D activation of phosphatidylinositol 3-kinase (PI-3-K) and mitogen-activated protein extracellular signal-regulated kinase (MEK) signaling pathways, while G12C and G12V led to activated Ral signaling and decreased growth factor-dependent Akt activation, further demonstrating distinct downstream signaling dependent on the K-Ras G12 mutant state.[55] Exactly how the identity of the G12 substitution impacts downstream signaling is not yet well defined. Powis and co-workers used molecular modeling to suggest that different sizes of G12X substitutions differently impact how the K-Ras variants interact with their downstream partners, in this case PI-3-K or itself (homodimerization), which subsequently impacts RaLGDS binding.[55] Molecular modeling simulations of WT K-Ras and the G12D variant suggest additionally that more long-range effects could matter, and that the G12D substitution increases flexibility in three regions: the P-loop (residues 10−14), switch-1 (residues 27−36), and switch-2 (residues 58−64) regions. Empirical techniques to probe how mutations at the G12 position affect K-Ras conformation and flexibility would help to better elucidate the mechanisms behind differential binding affinity and selectivity.[56] By using UVPD-MS, we identified differences between mutant K-Ras proteins that are the same, or in close proximity (residues 15, 16, 41−48), to the long-range effects predicted by molecular modeling simulations.

Our empirical studies of structural variations in K-Ras complexes containing single mutations based on the UVPD fragmentation allows further speculation about how each mutation might differently modulate the interactions of K-Ras with effector proteins (like Raf) as well as influence dimerization of K-Ras which is thought to be essential for interaction with Raf dimers for downstream signaling.[57,58] For instance, UVPD fragmentation was suppressed for the G12C·GDPnP·Mg^{2+} complex relative to the G12C·GDP·Mg^{2+} complex at the α-helical interface region which involves α-helices C and D (residues 86−105 and 126−138).[58] While dimers were not probed directly in the present study, the suppression of UVPD in α-helices C and D for the G12C·GDPnP·Mg^{2+} complex may indicate a stabilization of the α-helical bundles in the monomer, potentially translating to a more stable α-helical dimer which is the putative arrangement adopted for interaction with dimerized Raf.[58] In contrast, UVPD is suppressed in the effector region of the G12V·GDPnP·Mg^{2+} complex (relative to G12V·GDP·Mg^{2+}) which includes the β sheet region (such as residues 41−45 of β-strand B) and Switch I (residues 27−36) which form the β-interface. While the β-interface dimer is not the ideal homodimer for downstream signaling, evidence for higher order oligomerization states (Ras nanoclusters), most likely mediated through multiple interfaces, has been observed and suggested to be an important determinant in signaling output and fidelity.[55] For the third mutant probed (G12S), the increase in UVPD fragmentation at the P-loop (residues 8−15), switch I (residues 29−33), and β-strand B (residues 37−45) of the G12S·GDPnP·Mg^{2+} complex (relative to G12S·GDP·Mg^{2+}) suggests an increase in flexibility at the β-strand region in comparison to the G12V and G12C mutants. This overall increase in flexibility may serve a dual function to block effector binding and additionally to suppress the dimerization at the β-interface which is the incorrect orientation for Raf signaling.[58] Although further studies will be required to fully characterize the impact of each mutation on K-Ras binding partners, the UVPD-MS strategy clearly reveals the impact single amino acid changes at the G12X position have on protein conformation and flexibility, including long-range effects on protein structure. Experimental methods such as UVPD that provide this level of structural detail will be valuable in elucidating the causal links between changes in K-Ras protein structure and dynamics, mutant specific binding interactions, and the signaling phenotypes produced. Eventually, evaluation of other less studied K-Ras G12 mutants could have the potential to identify common fragmentation patterns shared between mutants that may prove to be prognostic of mutant specific signaling phenotypes.

CONCLUSION

The mutation of K-Ras at the 12th residue from glycine to cysteine, serine, or valine was successfully probed by UVPD-MS based on comparisons of backbone fragmentation efficiencies of complexes containing GDP or GDPnP for all K-Ras protein variants. Overall, the changes in UVPD fragmentation efficiencies reflect changes in protein conformation that are consistent with crystallographic or other experimental data and in fact provides a level of structural sensitivity not offered by many other biophysical approaches. The changes in backbone cleavage efficiencies are attributed to variations in the flexibility or rigidity of the protein in specific regions, primarily due to variations in intra- or intermolecular interactions that are sensitive to single point mutations. A series of holo product ions generated by UVPD offered a convenient means to map the GDP or GDPnP binding residues of K-Ras and also indicated that residues 121−125 interacted with the guanine portion of GDP or GDPnP. There was a notable increase in the UVPD backbone cleavage efficiency within the first 50 residues of K-Ras upon replacement of GDP by GDPnP, while at the same time there was a decrease in backbone cleavage efficiency in the region beyond the 100th residue. These two regions are known to interact with the phosphate and guanine portions, respectively, suggesting a shift in the binding motif upon the GDP/GDPnP ligand exchange. Most importantly, the series of G12X mutations resulted in unique changes in UVPD fragmentation of the K-Ras constructs that were significantly different upon ligand exchange. Interestingly, similarities were seen between hydrogen-bonding amino acid substitutions (C, S) and the bulkier substitution (V). This finding suggests a mechanism that links different K-Ras mutations to their resulting different downstream effects through long-range conformational or dynamic changes induced by the mutation. UVPD has proven to be a novel structural tool for probing G12X K-Ras mutations and should be easily applied to other positional isomers of K-Ras.

ASSOCIATED CONTENT

Supporting Information

The Supporting Information is available free of charge on the ACS Publications website at DOI: 10.1021/jacs.6b04474.

DOI: 10.1021/jacs.6b04474
J. Am. Chem. Soc. 2016, 138, 13187−13196

Discussion of protein expression and purification and K-Ras nucleotide exchange; Figures S1−12, showing color-coded diagrams of the crystal structure of K-Ras to facilitate identification of structural elements, ESI and UVPD mass spectra of the K-Ras complexes, a graph showing the average mass shift associated with complexation of the GDP or GDPnP ligands, expanded regions of the UVPD fragmentation trends of the complexes, several graphical displays of statistical treatments used to assess the UVPD data, and a graphical display illustrating the establishment of significance for the variations in backbone cleavage efficiencies; Tables S1−S8, summarizing all product ions identified upon UVPD of the various K-Ras complexes, and Table S9, summarizing residues for which UVPD is enhanced or suppressed for each complex (PDF)

AUTHOR INFORMATION

Corresponding Author

*jbrodbelt@cm.utexas.edu

Notes

The authors declare no competing financial interest.

ACKNOWLEDGMENTS

We thank Daniel Gentile and Kevan Shokat (University of California, San Francisco) for a generous gift of the WT and G12C K-Ras expression plasmids. This work was supported in part by grants from the National Science Foundation (NSF) (CHE-1402753) and the Robert A. Welch Foundation (F-1155 to J.S.B. and F-1572 to W.F.). Additionally, M.B.C. acknowledges Agilent for the sponsorship of the Division of Analytical Chemistry ACS fellowship.

REFERENCES

(1) Erichsen, H. C.; Chanock, S. J. *Br. J. Cancer* **2004**, *90* (4), 747−751.
(2) Rebbeck, T. R.; Ambrosone, C. B.; Bell, D. A.; Chanock, S. J.; Hayes, R. B.; Kadlubar, F. F.; Thomas, D. C. *Cancer Epidemiol., Biomarkers Prev.* **2004**, *13* (5), 681−687.
(3) Colicelli, J. *Sci. Signaling* **2004**, *2004* (250), RE13.
(4) Prior, I. A.; Lewis, P. D.; Mattos, C. *Cancer Res.* **2012**, *72* (10), 2457−2467.
(5) Konermann, L.; Vahidi, S.; Sowole, M. A. *Anal. Chem.* **2014**, *86* (1), 213−232.
(6) Miteva, Y. V.; Budayeva, H. G.; Cristea, I. M. *Anal. Chem.* **2013**, *85* (2), 749−768.
(7) Ngounou Wetie, A. G.; Sokolowska, I.; Woods, A. G.; Roy, U.; Loo, J. A.; Darie, C. C. *Proteomics* **2013**, *13* (3−4), 538−557.
(8) Pirrone, G. F.; Iacob, R. E.; Engen, J. R. *Anal. Chem.* **2015**, *87* (1), 99−118.
(9) Mendoza, V. L.; Vachet, R. W. *Mass Spectrom. Rev.* **2009**, *28* (5), 785−815.
(10) Fitzgerald, M. C.; West, G. M. *J. Am. Soc. Mass Spectrom.* **2009**, *20* (6), 1193−1206.
(11) Engen, J. R. *Anal. Chem.* **2009**, *81* (19), 7870−7875.
(12) Konermann, L.; Pan, J.; Liu, Y.-H. *Chem. Soc. Rev.* **2011**, *40* (3), 1224−1234.
(13) Sharon, M.; Robinson, C. V. *Annu. Rev. Biochem.* **2007**, *76* (1), 167−193.
(14) Heck, A. J. R. *Nat. Methods* **2008**, *5* (11), 927−933.
(15) Ben-Nissan, G.; Sharon, M. *Chem. Soc. Rev.* **2011**, *40* (7), 3627−3637.
(16) Snijder, J.; Heck, A. J. R. *Annu. Rev. Anal. Chem.* **2014**, *7* (1), 43−64.
(17) Van Duijn, E. *J. Am. Soc. Mass Spectrom.* **2010**, *21* (6), 971−978.
(18) Vahidi, S.; Stocks, B. B.; Konermann, L. *Anal. Chem.* **2013**, *85* (21), 10471−10478.
(19) Konermann, L.; Ahadi, E.; Rodriguez, A. D.; Vahidi, S. *Anal. Chem.* **2013**, *85* (1), 2−9.
(20) Schennach, M.; Breuker, K. *Angew. Chem., Int. Ed.* **2014**, *53* (1), 164−168.
(21) Breuker, K.; Brüschweiler, S.; Tollinger, M. *Angew. Chem., Int. Ed.* **2011**, *50* (4), 873−877.
(22) McAllister, R. G.; Metwally, H.; Sun, Y.; Konermann, L. *J. Am. Chem. Soc.* **2015**, *137* (39), 12667−12676.
(23) Uetrecht, C.; Rose, R. J.; van Duijn, E.; Lorenzen, K.; Heck, A. J. R. *Chem. Soc. Rev.* **2010**, *39* (5), 1633−1655.
(24) Hopper, J. T. S.; Oldham, N. J. *J. Am. Soc. Mass Spectrom.* **2009**, *20* (10), 1851−1858.
(25) Jurneczko, E.; Barran, P. E. *Analyst* **2011**, *136* (1), 20−28.
(26) Niu, S.; Rabuck, J. N.; Ruotolo, B. T. *Curr. Opin. Chem. Biol.* **2013**, *17* (5), 809−817.
(27) Rose, R. J.; Damoc, E.; Denisov, E.; Makarov, A.; Heck, A. J. R. *Nat. Methods* **2012**, *9* (11), 1084−1086.
(28) Cubrilovic, D.; Barylyuk, K.; Hofmann, D.; Walczak, M. J.; Gräber, M.; Berg, T.; Wider, G.; Zenobi, R. *Chem. Sci.* **2014**, *5* (7), 2794−2803.
(29) Li, H.; Wongkongkathep, P.; Van Orden, S. L.; Ogorzalek Loo, R. R.; Loo, J. A. *J. Am. Soc. Mass Spectrom.* **2014**, *25* (12), 2060−2068.
(30) Cammarata, M. B.; Thyer, R.; Rosenberg, J.; Ellington, A.; Brodbelt, J. S. *J. Am. Chem. Soc.* **2015**, *137* (28), 9128−9135.
(31) Li, H.; Wolff, J. J.; Van Orden, S. L.; Loo, J. A. *Anal. Chem.* **2014**, *86* (1), 317−320.
(32) Cammarata, M. B.; Brodbelt, J. S. *Chem. Sci.* **2015**, *6* (2), 1324−1333.
(33) O'Brien, J. P.; Li, W.; Zhang, Y.; Brodbelt, J. S. *J. Am. Chem. Soc.* **2014**, *136* (37), 12920−12928.
(34) Zhang, Z.; Browne, S. J.; Vachet, R. W. *J. Am. Soc. Mass Spectrom.* **2014**, *25* (4), 604−613.
(35) Breuker, K.; Oh, H.; Horn, D. M.; Cerda, B. A.; McLafferty, F. W. *J. Am. Chem. Soc.* **2002**, *124* (22), 6407−6420.
(36) Breuker, K.; McLafferty, F. W. *Proc. Natl. Acad. Sci. U. S. A.* **2008**, *105* (47), 18145−18152.
(37) Zhang, H.; Cui, W.; Gross, M. L. *Int. J. Mass Spectrom.* **2013**, *354*−*355*, 288−291.
(38) Lermyte, F.; Konijnenberg, A.; Williams, J. P.; Brown, J. M.; Valkenborg, D.; Sobott, F. *J. Am. Soc. Mass Spectrom.* **2014**, *25* (3), 343−350.
(39) Zhang, H.; Cui, W.; Gross, M. L.; Blankenship, R. E. *FEBS Lett.* **2013**, *587* (8), 1012−1020.
(40) Blackwell, A. E.; Dodds, E. D.; Bandarian, V.; Wysocki, V. H. *Anal. Chem.* **2011**, *83* (8), 2862−2865.
(41) Zhou, M.; Jones, C. M.; Wysocki, V. H. *Anal. Chem.* **2013**, *85* (17), 8262−8267.
(42) Shaw, J. B.; Li, W.; Holden, D. D.; Zhang, Y.; Griep-Raming, J.; Fellers, R. T.; Early, B. P.; Thomas, P. M.; Kelleher, N. L.; Brodbelt, J. S. *J. Am. Chem. Soc.* **2013**, *135* (34), 12646−12651.
(43) Cannon, J. R.; Cammarata, M. B.; Robotham, S. A.; Cotham, V. C.; Shaw, J. B.; Fellers, R. T.; Early, B. P.; Thomas, P. M.; Kelleher, N. L.; Brodbelt, J. S. *Anal. Chem.* **2014**, *86* (4), 2185−2192.
(44) Cammarata, M.; Lin, K.-Y.; Pruet, J.; Liu, H.; Brodbelt, J. *Anal. Chem.* **2014**, *86* (5), 2534−2542.
(45) Warnke, S.; Baldauf, C.; Bowers, M. T.; Pagel, K.; von Helden, G. *J. Am. Chem. Soc.* **2014**, *136* (29), 10308−10314.
(46) Warnke, S.; von Helden, G.; Pagel, K. *Proteomics* **2015**, *15* (16), 2804−2812.
(47) Hunter, J. C.; Gurbani, D.; Ficarro, S. B.; Carrasco, M. A.; Lim, S. M.; Choi, H. G.; Xie, T.; Marto, J. A.; Chen, Z.; Gray, N. S.; Westover, K. D. *Proc. Natl. Acad. Sci. U. S. A.* **2014**, *111* (24), 8895−8900.
(48) Araki, M.; Shima, F.; Yoshikawa, Y.; Muraoka, S.; Ijiri, Y.; Nagahara, Y.; Shirono, T.; Kataoka, T.; Tamura, A. *J. Biol. Chem.* **2011**, *286* (45), 39644−39653.

DOI: 10.1021/jacs.6b04474
J. Am. Chem. Soc. 2016, 138, 13187−13196

(49) Lim, S. M.; Westover, K. D.; Ficarro, S. B.; Harrison, R. A.; Choi, H. G.; Pacold, M. E.; Carrasco, M.; Hunter, J.; Kim, N. D.; Xie, T.; Sim, T.; Jänne, P. A.; Meyerson, M.; Marto, J. A.; Engen, J. R.; Gray, N. S. *Angew. Chem., Int. Ed.* **2014**, *53* (1), 199−204.
(50) Lu, S.; Jang, H.; Muratcioglu, S.; Gursoy, A.; Keskin, O.; Nussinov, R.; Zhang, J. *Chem. Rev.* **2016**, *116* (11), 6607−6665.
(51) Ostrem, J. M.; Peters, U.; Sos, M. L.; Wells, J. A.; Shokat, K. M. *Nature* **2013**, *503* (7477), 548−551.
(52) Seeburg, P. H.; Colby, W. W.; Capon, D. J.; Goeddel, D. V.; Levinson, A. D. *Nature* **1984**, *312* (5989), 71−75.
(53) Scheffzek, K.; Ahmadian, M. R.; Kabsch, W.; Wiesmüller, L.; Lautwein, A.; Schmitz, F.; Wittinghofer, A. *Science* **1997**, *277* (5324), 333−339.
(54) Hammond, D. E.; Mageean, C. J.; Rusilowicz, E. V.; Wickenden, J. A.; Clague, M. J.; Prior, I. A. *J. Proteome Res.* **2015**, *14* (3), 1535−1546.
(55) Ihle, N. T.; Byers, L. A.; Kim, E. S.; Saintigny, P.; Lee, J. J.; Blumenschein, G. R.; Tsao, A.; Liu, S.; Larsen, J. E.; Wang, J.; Diao, L.; Coombes, K. R.; Chen, L.; Zhang, S.; Abdelmelek, M. F.; Tang, X.; Papadimitrakopoulou, V.; Minna, J. D.; Lippman, S. M.; Hong, W. K.; Herbst, R. S.; Wistuba, I. I.; Heymach, J. V.; Powis, G. *J. Natl. Cancer Inst.* **2012**, *104* (3), 228−239.
(56) Chen, C.-C.; Er, T.-K.; Liu, Y.-Y.; Hwang, J.-K.; Barrio, M. J.; Rodrigo, M.; Garcia-Toro, E.; Herreros-Villanueva, M. *PLoS One* **2013**, *8* (2), e55793.
(57) Freeman, A. K.; Ritt, D. A.; Morrison, D. K. *Small GTPases* **2013**, *4* (3), 180−185.
(58) Muratcioglu, S.; Chavan, T. S.; Freed, B. C.; Jang, H.; Khavrutskii, L.; Freed, R. N.; Dyba, M. A.; Stefanisko, K.; Tarasov, S. G.; Gursoy, A.; Keskin, O.; Tarasova, N. I.; Gaponenko, V.; Nussinov, R. *Structure* **2015**, *23* (7), 1325−1335.

DOI: 10.1021/jacs.6b04474
J. Am. Chem. Soc. 2016, 138, 13187−13196